Tissue Classification from CT of Liver Volumetric Dataset Using 3D Relational Features

Wan Nural Jawahir Hj Wan Yussof
Chair for Pattern Recognition and Image Processing
Albert-Ludwigs-Universität Freiburg
Freiburg im Breisgau, Germany
yussof@informatik.uni-freiburg.de

Hans Burkhardt
Chair for Pattern Recognition and Image Processing
Albert-Ludwigs-Universität Freiburg
Freiburg im Breisgau, Germany
Hans.Burkhardt@informatik.uni-freiburg.de

***Abstract*—This paper proposes an extension of two dimensional relational features into three dimensions. In two dimensions, the relational features are extracted using a non-linear kernel function. This function is applied to the values of the points of two circles. To extract 3D relational features, we represent the points on the two spheres. We aim at classifying the tissue from Computed Tomography (CT) of liver datasets into three classes; normal, abnormal and others(i.e., kidneys, blood vessel, etc.). For this task, 100 known points from 6 CT datasets were used for training using the Support Vector Machine (SVM) classifier and 150 points from 10 CT datasets were used for validation. The results presented in this paper show that the relational features are promising.**

***Keywords*-invariant features, relational kernels, Computed Tomography (CT);**

I. INTRODUCTION

Image data contains meaningful information that has to be automatically extracted using computers or electronic devices. Such image information are called image features. Depending upon the particular task, the extracted features capture morphological properties, color properties, or certain textural properties of the image.

Based on the collection of texture definitions in [6], formulated by different vision researchers, it is difficult to express the true meaning of texture. However, the utilization of texture features is of increasing interest in many domains, including in the medical domain. Major categories of texture can be grouped into three subfields: texture segmentation, texture classification and texture synthesis. Texture segmentation works on partitioning the differently textured regions in an image. Taking advantage of structural content from a small digital sample image, one can construct a large image. This process is called texture synthesis. In texture classification, the goal is to assign an unknown sample image to one of the known texture classes. We attract the attention of the reader to [6], as these categories have already been discussed in detail by the authors.

This paper deals with the classification problem and presents a method for distinguishing normal tissue from abnormal tissue based on three dimensional textures using CT data recordings of liver datasets. The organization of this paper is as follows: In Section 2, we will review the role of texture features used in medical image processing. In Section 3, we describe the proposed texture feature. Section 4 presents and discusses the results and finally we give the conclusion in Section 5.

II. TEXTURE FEATURES IN MEDICAL APPLICATIONS

Texture features have been applied in many medical image analysis and computer vision problems [1][2][11]. In general, the applications involve the automatic feature extraction from the image. The features are then used for a variety of medical tasks such as classification, segmentation, registration and medical images indexing and retrieval.

Kovalev et al. [11] proposed an extended co-occurrence descriptor for three dimensional texture analysis of MRI datasets. The method is based on extended multi-sort co-occurrence matrices that combine intensity, gradient and anisotropy image features. They have demonstrated that their method is an efficient tool in various MRI image analysis tasks such as classification of brain datasets and segmentation of diffuse brain lesions.

For the registration task, Jarc et al. [1] extracted Laws texture coefficients and used them for computing registration criterion functions. The purpose of their work is to analyze the importance of texture information for registration of a digitaly reconstructed radiograph (DRR) and medical electronic portal image (EPI). They computed a registration criterion function directly from the intensity values, i.e., gray-values, for comparison to their proposed feature based approach. Three observations have been done; the accuracy of registration, the distinctiveness of local extrema and the distinctiveness of a global extrema of the criterion functions. These parameters are essential to achieve a correct image alignment. From the given image modalities, a more robust and correct registration can be expected using texture based instead of using intensity based criterion functions.

Manduca et al. [2] used texture features for the prediction of breast cancer from mammographic images. They extracted five textural features. For each image, a total of 1,050 Markovian texture features, 112 run length features,

 ISBN: 978-1-61208-111-3

250 Laws features and 30 Wavelet features were extracted from the central area of the breast where the thickness is nearly uniform and is referred as constant thickness region (CTR). A total of 41 Fourier features were calculated within the CTR-box. The CTR-box was obtained from the largest rectangular box that can be inscribed within the breast region. For the evaluation they used 381 datasets for training and 387 datasets for validation. The results consistently show that texture features at low spatial frequencies provided the strongest predictors of future breast cancer risk.

Tesar et al. [4] proposed a texture-based segmentation of organs for disease diagnostic. They proposed the extension of 2D Haralick texture features to 3D. For this work, they calculated a separate co-occurrence matrix for each voxel in the 3D image. The co-occurrence matrix is calculated from all voxels in a small rectangular window around the voxel. This makes it possible to segment given a 3D image as opposed to calculating the feature for the pre-segmented regions of an image. Consequently, such features can be used to search for very small regions with different texture properties (like tumors). A set of abdomen CT images was used for evaluation of the proposed approach. They used a Gaussian Mixture Model for the segmentation and for learning the parameters of the mixture models from the training dataset, an expectation-maximization (EM) approach was used.

In medical retrieval applications, Glatard et al. [9] used a bank of Gabor filters, one of the most popular texture features for medical image indexing and retrieval with a database of a cardiac magnetic resonance images. Each filter was tuned to a specific orientation and spatial frequency. Gabor filters with an angular spacing of 30° (corresponding to the orientations $0^\circ, 30^\circ, 60^\circ, 90^\circ, 120^\circ$ and 150°) and a frequency spacing of one octave (corresponding to the frequencies $\sqrt{2}, 2\sqrt{2}, ..., \frac{N}{4}\sqrt{2}$ cycles per image, N being the size of the image) were calculated. 42 Gabor filters were used for image indexing and 16 Gabor filters were used for segmentation assisted retrieval.

We discovered from the literature review that texture features are an important property in many medical applications. However, among texture features, relational features have not received much attention in this field. In this paper, our intention is to expose the potential of the proposed texture features to the researchers who are enthusiastic in medical image analysis.

III. Relational Invariant Features

In this work, we focus on the classification of liver tissue from datasets based on extended relational features. These features have been successfully used in the SIMBA (Search IMages By Appearance) system[1]. The advantage of using this method is that it is insensitive to image noise and also invariant to a group of image transformations

[1]http://simba.informatik.uni-freiburg.de/

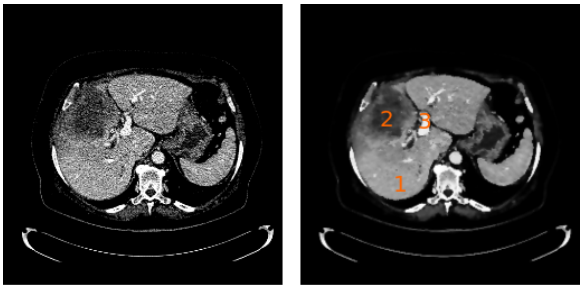

Figure 1. CT scans showing the low-density metastases in the upper right lobe of the liver. These tissues are labeled as 2 (abnormal). The blood vessels which are labeled as 3 (others) also appear as if they have been enhanced with contrast media and are brighter than 1 (normal) liver tissues. Image on the right is the result after noise filtering using anisotropic diffusion from raw data on the left.

(e.g.,translation and rotation). Using a slice-by-slice two-dimensional approach is still possible but it suffers from the drawback of some important information loss. To benefit from all information in 3D space, we extend the relational features to three dimensions. Note that, since CT data normally comes with low resolution and high noise, our method does not directly work on a raw volume data. We filtered the data using 3D anisotropic diffusion (see Figure 1).

A. Invariant Features

In two dimensions, a gray value image, X are represented as $X(x, y), (0 \leq x < M, 0 \leq y < N)$ with $X(x, y)$ be the gray-value at pixel coordinate (x, y) and MxN is the image domain. Let $\mathcal{G}$ be the transformation group of translation and rotation with elements $g \in \mathcal{G}$ acting on the images. The transformed images are gX. An invariant feature must satisfy $F(gX) = F(X), \forall g \in \mathcal{G}$. Integrating $f(gX)$ over the transformation group $\mathcal{G}$ constructs such invariant features as follows:

$$I(X) = \frac{1}{|\mathcal{G}|} \int_{\mathcal{G}} f(gX) dg \tag{1}$$

Eq. 1 becomes

$$\mathrm{IF}(X) = \frac{1}{2\pi MN} \int_{x=0}^{M} \int_{y=0}^{N} \int_{\theta=0}^{2\pi} f(g(x, y, \theta)X) d\theta dx dy \tag{2}$$

when applying the integration over all possible rotations and translations (Haar integral over the Euclidean motion). In discrete form the Eq. 2 is defined as:

$$\mathrm{IF}(X) \approx \frac{1}{qMN} \sum_{x=0}^{M-1} \sum_{y=0}^{N-1} \sum_{j=0}^{q-1} f(g(x, y, \theta = j\frac{2\pi}{q})X) \tag{3}$$

where IF is approximated by choosing x and y to be integers and by varying θ in a discrete manner producing q samples. Interpolation is used to solve the problem of points that do not lie on the image grid.

 ISBN: 978-1-61208-111-3

As can be observed, Eq. 3 can be computed locally by applying the kernel function f, on the neighborhood of each pixel in the image for all possible values of θ.

$$\mathrm{IF}_{\mathrm{local}}(x,y) = \frac{1}{q}\sum_{j=0}^{q-1}(f(g(x,y,\theta = j\frac{2\pi}{q})X)). \quad (4)$$

The summation over the angle θ can be replaced with histogramming [8].

$$\mathrm{IF}_{\mathrm{local}}(x,y) = \mathrm{hist}(f(g(x,y,\theta = j\frac{2\pi}{q})X)), j = 0,...,q-1. \quad (5)$$

In this way, local information can be preserved and thus increasing the discrimination capabilities of features.

B. Relational Features

The relational features are calculated similar to Local Binary Pattern (LBP) texture features [10]. LBP thresholds the neighborhood with the gray value of its center pixel and represents the result as a binary pattern (0 and 1). Applying this to all pixels in a circular neighborhood of the center pixel, the binary pattern is then transformed into a unique number as follows:

$$\mathrm{LBP} = \sum_{i=0}^{n-1} s(v_i - v_c)2^i, \text{where} \quad (6)$$

$$s(x) = \begin{cases} 1 & x \geq 0, \\ 0 & x < 0 \end{cases} \quad (7)$$

where v_i and v_c are the gray values at a neighboring pixel and at the center pixel, respectively. The number of the pixels in the circular neighborhood is denoted by n. The drawback of LBP is that the discontinuity of the LBP operator (the s function), since it maps to 0 or 1 which makes them sensitive to noise. A small disturbance in the image may cause a big deviation of the feature.

Using the following form

$$f(X) = \mathrm{rel}(X(x_1,y_1) - X(x_2,y_2)) \quad (8)$$

we construct an invariant feature by applying Eq. 8 onto Eq. 4. Schael [5] has introduced a ramp function that extends the step function in Eq. 7 giving values in the range of $[0,1]$ as follows:

$$\mathrm{rel}(\eta) = \begin{cases} 1 & \text{if } \eta < -\varepsilon \\ \frac{\varepsilon-\eta}{2\varepsilon} & \text{if } -\varepsilon \leq \eta \leq \varepsilon \\ 0 & \text{if } \varepsilon < \eta \end{cases} \quad (9)$$

where ε is a threshold parameter. Using a ramp function, it is now more robust to image noise. Note that, if ε is set to zero, then the rel function will reduce to the simple LBP operator s.

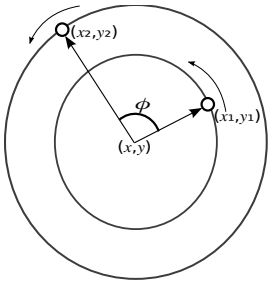

Figure 2. Calculation of a set of relational features in two dimensions. A feature is formed by applying the relational function to the gray-value difference of the pixels lying on the specific distance and phase to the reference point (i.e. center of the circles)

As opposed to LBP, 2D relational features use two circular sets. Let (x,y) be the coordinates of central pixel in two-dimension, taking into consideration a phase shift, ϕ, the coordinates (x_1,y_1) and (x_2,y_2) in Eq. 8 are given by:

$$(x_1,y_1) = (x + r_1\cos(\theta), y + r_1\sin(\theta)) \quad (10)$$

$$(x_2,y_2) = (x + r_2\cos(\theta+\phi), y + r_2\sin(\theta+\phi)) \quad (11)$$

where r_1 and r_2 are the radii of the first and second circle, respectively. Local information at different scales and orientations can be captured with different combinations of r_1, r_2 and ϕ. The calculation of two dimensional relational features is illustrated in Figure 2

C. Extension Relational Features to Three Dimension

In this paper, we present an extension of relational features to three dimensions. The relational function in Eq. 8 for three dimensions is very straightforward and is given by:

$$f(X) = \mathrm{rel}(X(x_1,y_1,z_1) - X(x_2,y_2,z_2)) \quad (12)$$

We have seen that LBP and 2D relational features use circular sets to represent the neighborhood of a central pixel. To extent relational features to three dimensions, a logical way is to represent neighbors in unit sphere. Thus for a central voxel with the coordinates (x,y,z), the coordinates of (x_1,y_1,z_1) and (x_2,y_2,z_2) are given by:

$$(x_1,y_1,z_1) = (x + r_1\cos(\theta)\sin(\psi), \\ y + r_1\sin(\theta)\sin(\psi), z + r_1\cos(\psi)) \quad (13)$$

$$(x_2,y_2,z_2) = (x + r_2\cos(\theta+\phi_1)\sin(\psi+\phi_2), \\ y + r_2\sin(\theta+\phi_1)\sin(\psi+\phi_2), z + r_2\cos(\psi+\phi_2)) \quad (14)$$

where ϕ_1 and ϕ_2 denote the phase shifts, between the corresponding points (x_1,y_1,z_1) and (x_2,y_2,z_2).

Given n set of parameters with $i = 0,\ldots,n$, we define our three dimensional relational features, $\mathrm{R}(x,y,z,r_1,r_2,\phi_1,\phi_2,q)$, calculated on a local point (x,y,z) as follows:

$$\mathrm{RF}_i = [\mathrm{R}(x,y,z,r_1,r_2,\phi_1,\phi_2,q)]_i \\ \mathrm{RF}_i = \mathrm{rel}(X(x_1,y_1,z_1) - X(x_2,y_2,z_2)) \quad (15)$$

 ISBN: 978-1-61208-111-3

Three dimensional invariant features in Eq. 4 becomes

$$\mathrm{IF}_{local}(i)|_{(x,y,z)} = \mathrm{hist}(f_i(x,y,z,\theta,\psi)X)), \qquad (16)$$

where θ is an azimuthal coordinate running from 0 to 2π (longitude) and ψ is a polar coordinate running from 0 to π (colatitude). We end up with one dimensional feature vector with t bins.

IV. Results

For the evaluation of our three dimensional relational features, 100 training points from 6 CT datasets and 150 test points from 10 CT datasets were used for the classification task. These points are labeled as 1 (normal tissue), 2 (abnormal tissue) and 3 (others, i.e., blood vessels, kidneys that could not be removed during segmentation). The Support Vector Machine (SVM) classifier[2] was used for the classification task. Three tests were conducted in this work. As SVM kernel, we used the radial basis function (RBF) kernel for the classification task with a pair of parameters (C, γ). Here, C denotes the cost value that penalizes misclassifications and γ is the width-parameter in the RBF kernel.

We used four sets of parameters, $(r_1 = 0, r_2 = 5, \phi_1 = 0)$, $(r_1 = 2, r_2 = 3, \phi_1 = \pi/4)$, $(r_1 = 3, r_2 = 6, \phi_1 = \pi/2)$ and $(r_1 = 4, r_2 = 8, \phi_1 = \pi)$, each with $q = 20$. For all tests, we set $\phi_2 = 0$. This means only on longitude direction a phase shift was applied. The rel threshold, $\varepsilon = 0.196$ was used. At each point, we obtained $20 * 4 = 80$ features. Histogram relational features (hRF) were divided into 20 bins. The length of feature vector was reduced to 20.

For the first test, we set $C = 1000$ and $\gamma = 0.02$. hRF attains an accuracy of 86.67% for this test. Table I shows the confusion matrix with the true positive (TP) and false positive (FP) of the first test. 71 out of 79 are correctly classified as class 1 given 89.87% of TP and 7 out of 71 tissues from class 2 and 3 are incorrectly identified as class 1 given 9.859% of FP. The TP and FP for class 2 are 93.1% and 7.438%, respectively. However, the TP for class 3 is quite low (76.19%) since this class consists of several different tissues, which might have different tissue structures. Only 3.704% of tissues from class 1 and 2 are wrongly classified as class 3.

Table I
Confusion matrix and true positive (TP) and false positive (FP) for the three category classification task

%	1	2	3	TP	FP
1	**71**	6	2	71/79 (89.87%)	7/71 (9.859%)
2	0	**27**	2	27/29 (93.1%)	9/121 (7.438%)
3	7	3	**32**	32/42 (69.05%)	4/108 (3.704%)
total :				130/150 (86.67%)	20/150 (13.33%)

In the second and third tests, we compared the result of hRF with relational features that were computed by averaging. We refer to the features as aRF. We also compared the results with the gray-level co-occurrence matrix (GLCM) texture features [7] and Gabor wavelets [3]. We used the same SVM kernel as the first test for the classification. The GLCMs and Gabor wavelets used in this study were also extracted in 3D space.

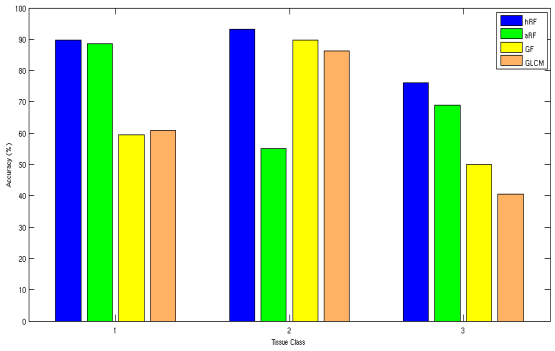

Figure 3. Comparison of the proposed texture features with 3D GLCM and 3D Gabor wavelets for the accuracy of different tissue classes.

Eight Haralick statistic measurements to describe the 3D GLCM were calculated using a window size of 5x5x5 in 13 directions$((0°, 45°)$, $(0°, 90°)$, $(0°, 135°)$, $(45°, 45°)$, $(45°, 90°)$, $(45°, 135°)$, $(90°, 45°)$, $(90°, 90°)$,$(90°, 135°)$, $(135°, 45°)$, $(135°, 90°)$, $(135°, 135°)$ and $(-, 0°))$ for contrast, homogeneity, angular second moment, entropy, maximum probability, energy and correlation measurements. 3D Gabor wavelets used in this study follow the formula given in [3]. A set of Gabor wavelets of different frequencies f_i and orientations (θ_j, ϕ_k) was calculated with the following representation:

$$\{\psi_{f_i,\theta_j,\phi_k(x,y,z)}, f_i = 0.5/(\sqrt{2})^i, \theta_j = j\pi/J, \phi_k = k\pi/K\} \qquad (17)$$

A window size of 25x25x25 was used to produce Gabor filters and convolved with the same size of sub-image with point being evaluated was located at the center of the sub-image. The mean of convolution result was used to represent Gabor feature. Since a set of Gabor wavelets $\{\psi_{f_i,\theta_j,\phi_k}\}$ was used, IxJxK length of feature vector were obtained with $i = 0, ..., I-1$, $j = 0, ..., J-1$ and $k = 0, ..., K-1$. We set $I = J = K = 3$. This produced a total of 27 Gabor features (GF).

We performed the second test for comparison of classification accuracy for every class. On average, hRF outperforms GLCM by 26.67% and GF by 24%. aRF attains an accuracy of 80.67% in which hRF is better than aRF by 10%. See the graph in Figure 3 for comparison. It can be seen from the graph, the accuracy of GLCM and GF for class 1 and class 3 are worse than relational features. For class 2, aRF is the worst among all. However, hRF obtains the highest accuracy for all classes.

In the third test, we have computed the accuracy of

[2]http://lmb/lmbsoft/libsvmtl/svmtl.en.html

 ISBN: 978-1-61208-111-3

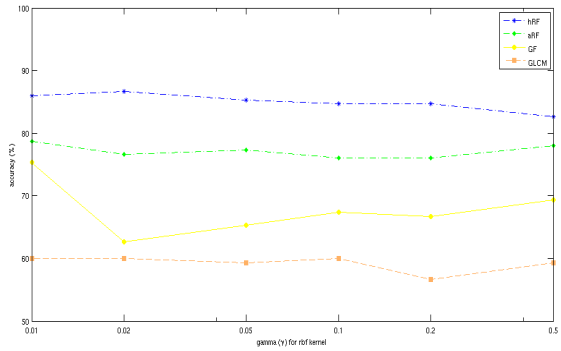

Figure 4. The accuracy of 3D relational features, 3D GLCM and 3D Gabor wavelets using different γ with $C = 1000$.

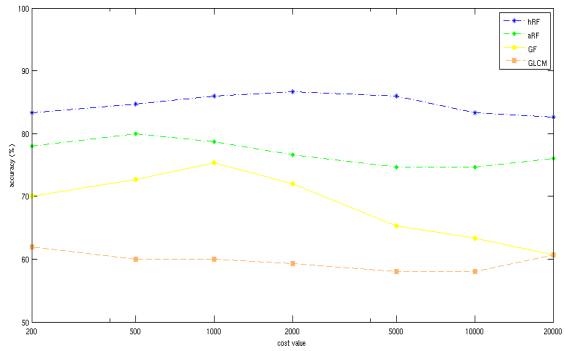

Figure 5. The accuracy of 3D relational features, 3D GLCM and 3D Gabor wavelets using different cost values, C with $\gamma = 0.01$.

all features using different pair of parameters (C, γ) for the RBF kernel. The result presented in Figure 4 was obtained by setting $\gamma = \{0.01, 0.02, 0.05, 0.1, 0.2, 0.5\}$ and $C = 1000$. In Figure 5, γ was set with 0.01 and $C = \{200, 500, 1000, 2000, 5000, 10000, 20000\}$. The results from both figures show that the relational features outperform GLCM and GF on the task. As predicted, hRF shows higher classification accuracy than aRF for all pair of parameters (C, γ) used in this test.

V. Conclusion and Future Work

In this paper, we proposed an extension of relational features to three dimensions. The purpose of this extension is to extract texture features from CT volumetric dataset to benefit from the full 3D information. The results from our study showed that the relational features achieved higher accuracy than the GLCMs and Gabor wavelets texture features in classifying different types of liver tissue from CT datasets. This indicated that, 3D relational features, especially hRF are promising for many medical applications that exploit texture features. For future work, we will consider nearby points to progress in the accuracy of liver tissue classification.

Acknowledgment

We would like to thank all the five anonymous reviewers for their helpful comments. We also immensely grateful to our colleague, Thorsten Schmidt for his comments and suggestions on an earlier version of this paper. The work has been partially sponsored by KPT/UMT under SLAI scheme.

References

[1] A. Jarc, P. Rogelj and S. Kovacic, *Texture Feature Based Image Registration* Biomedical Imaging: From Nano to Macro, 2007. ISBI 2007. 4th IEEE International Symposium on , vol., no., pp.17-20, 12-15 April 2007.

[2] A. Manduc, M. J. Carston, J. J. Heine, C. G. Scott, V. S. Pankratz, K. R. Brandt, T. A. Sellers, C. M. Vachon and J. R. Cerhan, *Texture Features from Mammographic Images and Risk of Breast Cancer*, Cancer Epidemiol Biomarkers Prev 2009, vol. 18(3), pp. 837–845, 2009.

[3] L. Shen and L. Bai, *3D Gabor wavelets for evaluating SPM normalization algorithm*, Medical Image Analysis, vol. 12, pp. 375–383, 2008.

[4] L. Tesar, D. Smutek, A. Shimizu and H. Kobatake, *3D Extension of Haralick Texture Features for Medical Image Analysis*

[5] M. Schael, *Invariant grey scale features for texture analysis based on group averaging with relational kernel function*., Internal Report 01/01, University of Freiburg, 2001.

[6] M. Tuceryan and A. K. Jain, *Texture Analysis*, The Handbook of Pattern Recognition and Computer Vision (2nd. Eds.) by C. H. Chen, L. F. Pau and P. S. P. Wang (eds.), pp. 207–248, World Scientific Publishing Co., 1998.

[7] R. M. Haralick, K. Shanmugam and I. Dinstein, *Textural Features for Image Classification*, IEEE Transactions on Systems, Man, and Cybernatics SMC(6), pp. 610–621, 1973.

[8] S. Siggelkow, M. Schael and H. Burkhardt, *SIMBA - Search IMages By Appearance*, DAGM, LNCS 2191, pp. 9–16, 2001.

[9] T. Glatard, J. Montagnat and I. E. Magnin, *Texture based medical image indexing and retrieval: application to cardiac imaging*, Proceedings of the 6th ACM SIGMM international workshop on Multimedia information retrieval, pp. 135–142, 2004.

[10] T. Ojala, M. Pietikäinen and T. Mäenpää, *Gray scale and rotation invariant texture classification with local binary patterns*. In Proceedings of the 6th European Conference on Computer Vision, pp. 404–420, 2000.

[11] V. A. Kovalev, F. Kruggel, H. J. Gertz and D. Y. von Cramon, *Three-dimensional Texture Analysis of MRI Brain Datasets*, IEEE Transactions on Medical Imaging, vol. 20(5), pp. 424–433, 2001.

 ISBN: 978-1-61208-111-3